Dephasing with strings attached

Claudio Castelnovo,[1,*] Mark I. Dykman,[2] Vadim N. Smelyanskiy,[3] Roderich Moessner,[4] and Leonid P. Pryadko[5,†]

[1] *T.C.M. Group, Cavendish Laboratory, University of Cambridge, J. J. Thomson Avenue, Cambridge CB3 0HE, U.K.*
[2] *Department of Physics and Astronomy, Michigan State University, East Lansing, Michigan 48824, USA*
[3] *Google Inc., Venice, California 90291, USA*
[4] *Max-Planck-Institut für Physik komplexer Systeme, 01187 Dresden, Germany*
[5] *Department of Physics & Astronomy, University of California, Riverside, California 92521, USA*

(Dated: November 9, 2017)

Motivated by the existence of mobile low-energy excitations like domain walls in one dimension or gauge-charged fractionalized particles in higher dimensions, we compare quantum dynamics in the presence of weak Markovian dephasing for a particle hopping on a chain and for an Ising domain wall whose motion leaves behind a string of flipped spins. Exact solutions show that the two models have near identical transport responses in the bulk. On the other hand, in finite-length chains, the broadening of discrete spectral lines is much more noticeable in the case of a domain wall. These results may be of relevance to a broad class of systems including quasi-1D antiferromagnets, polymer chains, and even retinal systems.

I. INTRODUCTION

The effect of environmental coupling on the time evolution is a fundamental issue in the study of open quantum systems. A classical example is *quantum diffusion* of point defects in crystalline helium. With coherent band width the smallest energy in the problem, of order 10^{-4}K, at low defect densities the diffusion coefficient is inversely proportional to the dephasing rate due to quasielastic phonon scattering[1–3]. The resulting temperature dependence has been confirmed in NMR experiments[4–6]. It was later realized by Andreev[7] that the same physics that governs the diffusive transport of microscopic defects—isotopic substitutions, adatoms, or vacancies—should also work for topological defects like kinks in a dislocation line.

The question we address in this work is what are the differences in macroscopic manifestation between these two cases—microscopic particles and topological excitations. The major microscopic difference is that the latter can act as a source of an observable emergent gauge field. A case in point is the dynamics of monopoles and Dirac strings[8,9] in spin ice[10].

Here we consider a simplified version of the spin ice setting, that discards the high-dimensional network of background spin configurations in favor of one-dimensional systems. This first pass at the problem enables us to contrast the motion of a free particle and that of a particle with a string attached, in the form of a domain wall in an Ising chain.

We solve and contrast these two cases, of particle and domain wall motion, subject to a locally uncorrelated Markovian dephasing bath. The main difference is that dephasing rates for far-off-diagonal elements of the density matrix are much higher for a domain wall, in agreement with the intuition from dephasing in an n-qubit quantum register[11]. Our solution demonstrates that, for unstructured motion in one dimension, the two cases differ only weakly, in the sense that the difference between the two is considerably smaller than the difference between either and the fully coherent time evolution. In particular, linear transport responses in the presence of a small density gradient or a weak uniform field are identical for the two cases, in perfect agreement with the insightful arguments by Andreev[7]. However, we notice that this is no longer the case when considering finite-length chains. Here, the discrete energy spectrum is broadened considerably more strongly for the case of domain walls. The effect is related to the enhanced fragility of the interference of a domain wall with itself when it does a round trip on the finite lattice to establish a standing wave.

One-dimensional and quasi-one-dimensional systems have been extensively studied experimentally for decades. Our results may be of direct relevance to a number of these. Examples we discuss below include the Villain mode[12] in $CsCoBr_3$ (Ref. 13), highly-tunable quantum simulators using both trapped ions[14] and cold atomic systems (where the Su-Schrieffer-Heeger model has been recently realised in momentum space[15]), and also solitons in polyacetylene and other molecular wires[16], as well as in retinal systems[17].

The remainder of this paper is structured as follows. In Sec. II, we introduce model, notations, and method. Sec III contains the main results of our work, for unbiased motion as well as in the presence of a dc or an ac driving field. Sec. IV is devoted to a discussion of the scope of experimental systems for which our analysis may be relevant, alongside a brief discussion of peculiarities of each of the set-ups in question. We conclude with an outlook in Sec. V. Further technical details are relegated to the Appendix A.

II. MODEL

The two models we solve describe one-dimensional hopping of a particle or a domain wall, respectively, in the presence of Markovian dephasing uncorrelated across

sites. Both models are conveniently expressed in terms of the density matrix with components ρ_{ab}, a and b being particle or domain wall position labels, via the equation

$$\dot{\rho}_{ab} = -i[H,\rho]_{ab} - \Gamma_{ab}\,\rho_{ab}. \quad \text{(no summation!)} \qquad (1)$$

The first term in the r.h.s. describes the Schrödinger evolution of the density matrix of a closed system. We take $H = H_0$ to be the usual hopping Hamiltonian with matrix elements

$$(H_0)_{ab} = -\frac{\Delta}{2}(\delta_{a,b+1} + \delta_{a+1,b}), \qquad (2)$$

where $\delta_{a,b}$ is the Kronecker symbol, and Δ denotes the half band width. For convenience we choose units where the lattice spacing and Planck's constant are set to 1.

The second term in the r.h.s. of Eq. (1) accounts for the coupling of the system to the external world. While generally such a coupling could result in a multitude of physical effects, we assume the regime dominated by Markovian dephasing. As we discuss below (and in more detail in the Appendix A) this limit is universal as long as the evolution of the density matrix remains slow on the scale of the bath correlation time, τ_c.

Central to our analysis is the difference in the dephasing rates for the off-diagonal elements of the density matrix in the two cases. For a hopping particle, the off-diagonal elements are all equal to each other,

$$\Gamma_{ab}^{(\mathrm{particle})} = \gamma\,(1-\delta_{a,b})\,. \qquad (3)$$

By contrast, the dephasing rates grow linearly with the distance from the diagonal in the case of a domain wall,

$$\Gamma_{ab}^{(\mathrm{dw})} = \gamma\,|a-b|\,. \qquad (4)$$

Here, γ is the dephasing rate scale.

At a formal level, Eqs. (1) and (3) can be considered a Lindblad equation[18,19] for single-particle hopping, in the case where each site has its own bath, see Fig. 1(a).

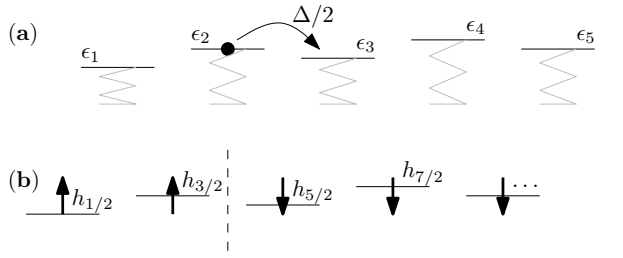

FIG. 1. The two models considered here: (a) A one-dimensional tight-binding model in the presence of dephasing caused by fluctuating energy levels $\epsilon_i \equiv \epsilon_i(t)$. (b) A domain wall in a ferromagnetic Ising chain in the presence of a transverse field and dephasing caused by fluctuating longitudinal magnetic fields $h_i \equiv h_i(t)$. The domain wall site is labelled by an integer index, and the spin positions are correspondingly half-integers.

Similarly, Eqs. (1) and (4) describe dynamics in a single-domain-wall sector of an Ising spin chain in the presence of the transverse field Δ and independently-fluctuating longitudinal magnetic fields, see Fig. 1(b). Shifting the domain wall by $|a-b|$ positions requires flipping $|a-b|$ spins, which in turn controls the dephasing rate for the matrix element ρ_{ab} (see, e.g., Ref. 11).

A. Discussion of the approximations involved

The standard derivation given in the Appendix A assumes the case of an oscillator (phonon) bath, including both first- and second-order coupling terms which can be interpreted respectively as contributions due to phonon absorption/emission and phonon scattering. With first-order coupling, Markovian dephasing is obtained only in the special case where the spectral function of the bath coupling has a linear in frequency "Ohmic" form. On the contrary, at sufficiently high temperatures, a generic second-order phonon-coupling Hamiltonian always produces Markovian dephasing as a result of quasi-elastic scattering of high frequency phonons.

Our derivation shows that for the Markovian limit to apply one needs both the bath temperature β^{-1} and the cutoff frequency ω_c to be large compared to the coefficients of Eq. (1). Formally, the bath correlation time can be defined as $\tau_c \sim \max(\beta, \omega_c^{-1})$. The usual Markovian limit, $\tau_c \to 0$, implies an infinite bath temperature, $\beta_c \to 0$, and $\omega_c \to \infty$. Correspondingly, the only stationary solution of Eq. (1) with $\Gamma_{ab} > 0$ for $a \neq b$ is classical (density matrix purely diagonal), with uniform density distribution between the sites, independently of the structure of the Hamiltonian H_0.

When the on-site baths are not independent, as in the case of dephasing by higher-dimensional phonon modes, one generically expects Γ_{ab} to depend non-trivially on $|a-b|$ even in the case of a particle. However, with the correlation between the sites asymptotically vanishing with increasing distance, at large $|a-b|$, Γ_{ab} is expected to saturate in the case of a particle, and continue to grow linearly in the case of a domain wall.

In the case of a domain wall, the Markovian approximation necessarily breaks down at large enough $|a-b|$. This is not a concern, however, since far off-diagonal matrix elements ρ_{ab} decay to zero rapidly and are not expected to modify the conclusions obtained from our simplified Eqs. (1) and (4) when both $\Delta\,\tau_c$ and $\gamma\,\tau_c$ are small.

III. SOLUTIONS OF THE MASTER EQUATION

Here we construct exact and approximate solutions of the Markovian master equation (1). On an infinite uniform chain, it is convenient to make evident the translational invariance with respect to the center-of-mass coordinate, $R \equiv (a+b)/2$. Thus, we define a translationally-

invariant matrix $\Gamma_{ab} \equiv V_{a-b}$, where $V_0 = 0$, and $V_s = V_{-s} > 0$ is the dephasing rate for the s'th diagonal of the density matrix, $s \neq 0$. From the previous section, we have $V_s = \gamma\,(1 - \delta_{s,0})$ and $V_s = \gamma\,|s|$, the Markovian dephasing rates for a particle, Eq. (3), and a domain wall, Eq. (4). It is also convenient to write the commutator in Eq. (1) explicitly,

$$\dot\rho_{ab} = i\frac{\Delta}{2}\sum_{\pm}\left(\rho_{a\pm1\,b} - \rho_{a\,b\pm1}\right) - V_{a-b}\rho_{ab}. \qquad (5)$$

A. Stationary polynomial solutions

To derive the (quantum) diffusion coefficient from Eq. (5), one would look for stationary solutions with a linear density gradient. Here, we introduce a slightly more general *polynomial* ansatz,

$$\rho_{ab} = g_0(s) + Rg_1(s) + R^2 g_2(s) + \ldots + R^m g_m(s), \quad (6)$$

where, as before, $s = a - b$ and $R = (a + b)/2$. After substituting in Eq. (5) and collecting matching powers of R, we obtain the following coupled equations,

$$\dot g_\ell(s) + V_s g_\ell(s) = i\Delta\sum_j \binom{j}{\ell} 2^{\ell-j}\left[g_j(s+1) - g_j(s-1)\right], \quad (7)$$

where $0 \le \ell \le m$, and the summation is over values of j in the interval $\ell < j \le m$, with $j - \ell$ odd. In particular, for $\ell = m$, the r.h.s. is zero, so that $g_m(s)$ decays exponentially, consistent with the later result in Eq. (15). In the stationary limit, $t \to \infty$, only the diagonal element $g_m(s = 0)$ remains non-zero. The stationary equation for $\ell = m - 1$ reads

$$V_s g_{m-1}(s) = im\Delta[g_m(s+1) - g_m(s-1)] \qquad (8)$$

and it gives non-zero solutions only for $s = \pm1$. Similarly, for $\ell = m - 2$, we get

$$V_s g_{m-2}(s) = i(m-1)\Delta[g_{m-1}(s+1) - g_{m-1}(s-1)] \quad (9)$$

and $g_{m-2}(s)$ is non-zero only for $s \in \{-2, 0, 2\}$. While the subsequent equations are more complicated, the general result is that non-zero stationary values of $g_j(s)$ are limited to $|s| \le m - j$.

Thus, with a polynomial order-m form (6) of the density matrix, its stationary matrix elements beyond m-th diagonal are necessarily zero. More generally, this implies a rapid fall-off of the matrix elements with the distance from the diagonal, suggesting that the specific form of V_s at large s be not important. This limits the possible differences in dc transport properties between the cases of a particle and a domain wall, Eqs. (3) and (4).

In particular, for the density that depends on the distance linearly [first order polynomial in powers of R in Eq. (6)], stationary solutions of Eq. (5) are exactly tridiagonal. Explicitly, the off-diagonal matrix elements are proportional to the density gradient,

$$\rho_{a,a+1} = -\rho_{a+1,a} = i\frac{\Delta}{2\gamma}(\rho_{a+1,a+1} - \rho_{a,a}).$$

These are exactly the matrix elements that determine the hopping current between sites a and $a + 1$,

$$J_{a,a+1} = i\frac{\Delta}{2}\left[\rho_{a,a+1} - \rho_{a+1,a}\right]. \qquad (10)$$

Replacing finite differences with the derivatives times the lattice spacing d, and rescaling the density, we obtain the coefficient of quantum diffusion

$$D = \frac{\Delta^2 d^2}{2\gamma}, \qquad (11)$$

exactly the same for particles and the domain walls.

This result only requires that both Δ and γ be small compared to temperature (and the bath cut-off frequency), it does not really matter which of them is larger[3,7]. In other words, the mean free path during the dephasing time can be large or small compared to the lattice spacing. This is different from transport in disordered systems, where quasiparticle description is expected to apply only while the mean free path remains larger than the lattice spacing[20,21]. One can thus say that quantum diffusion (controlled by dephasing due to time-dependent fluctuations of the energy levels) is insensitive to the nominal Ioffe-Regel crossover.

With the help of the Einstein relation, from Eq. (11) we also conclude that the corresponding mobilities should also be identical. Thus, by probing the usual dc linear transport response, one will see no difference between a particle and a domain wall.

B. Exact solutions on an infinite chain

More general solutions of Eq. (5) can be obtained by introducing the Fourier transform

$$\rho_{ab} = \int \frac{dK}{2\pi} e^{iKR} e^{i\pi s/2}\phi_s(t, K), \quad s \equiv a - b, \qquad (12)$$

where the phase factor $e^{i\pi s/2}$ is introduced to make explicit the reflection symmetry, $s \to -s$, in Eq. (13) below. Fourier modes $\phi_s \equiv \phi_s(t, K)$ at different K are independent, except the required Hermiticity of ρ, $\phi_s^*(t, K) = \phi_{-s}(t, -K)$. They obey the equation:

$$\dot\phi_s = -iu_K(\phi_{s+1} + \phi_{s-1}) - V_s\phi_s, \qquad (13)$$

$$u_K \equiv \Delta\sin(K/2). \qquad (14)$$

This can be viewed as a Schrödinger equation on a chain of site label s, with an imaginary on-site potential $-iV_s$.

With $K = 0$, the hopping (14) is zero, and the master equation (13) separates into a set of independent equations for each s. The corresponding solution reads

$$\phi_s(t, K = 0) = \phi_s(0, K = 0)\, e^{-V_s t}. \tag{15}$$

This is a special case $m = 0$ of the general polynomial in R solution derived in Sec. III A. Since $V_s = 0$ for $s = 0$, and positive otherwise, the resulting stationary solution is a purely diagonal classical density matrix, with density distributed uniformly along the chain, as would be expected at large temperatures.

1. Dynamics of a single particle

Let us now consider the master equation (13) for a general K in the case of a particle, $V_s = \gamma\,(1 - \delta_{s,0})$. This imaginary potential is a constant except for $s = 0$, which allows us to construct a solution for general initial conditions in quadratures using a version of the single-site scattering expansion. We start by writing a Laplace-transformed version of Eq. (13),

$$p\psi_s - \phi_s(0) = -iu_K(\psi_{s+1} + \psi_{s-1}) - \gamma\psi_s + \gamma\delta_{s,0}\psi_0, \tag{16}$$

where $\psi_s \equiv \psi_s(p, K) = \mathcal{L}\,[\phi_s(t, K)]$ is the Laplace transform of $\phi_s(t, K)$. Denote Q_s the Green's function (GF) of the translationally-invariant version of Eq. (16), the solution of this equation with the last term dropped, and $\phi_s(0) \equiv \phi_s(0, K)$ replaced by $\delta_{s,0}$,

$$Q_s = \int_0^{2\pi} \frac{dq}{2\pi} \frac{e^{iqs}}{p + \gamma + 2iu_K \cos q} \tag{17}$$

$$= \frac{e^{i\pi|s|/2}\big[y\big(\frac{p+\gamma}{2u_K}\big)\big]^{|s|}}{[(p+\gamma)^2 + 4u_K^2]^{1/2}}, \quad y(x) \equiv x - \sqrt{1 + x^2}, \tag{18}$$

where we need to select the branch with the square root positive at $p + \gamma > 0$. Then, the GF $G_{ss'}(p, K)$ of the full Eq. (16)—its solution with $\phi_s(0)$ replaced by $\delta_{ss'}$—is given by the multiple scattering series,

$$G_{ss'}(p, K) = Q_{s-s'} + Q_s\gamma Q_{-s'} + Q_s\gamma Q_0\gamma Q_{-s'} + \ldots$$

$$= Q_{s-s'} + \frac{Q_s\gamma\, Q_{-s'}}{1 - \gamma Q_0}. \tag{19}$$

In particular, the diagonal-to-diagonal matrix element,

$$G_{00}(p, K) = \frac{1}{[(p+\gamma)^2 + 4u_K^2]^{1/2} - \gamma}, \tag{20}$$

is the spatial Fourier/temporal Laplace transform of the probability $P \equiv P(R, t)$ for a particle initially at the origin to travel to site R in time t:

$$P = \int\limits_{\epsilon - i\infty}^{\epsilon + i\infty} \frac{dp}{2\pi i}\, e^{pt} \int\limits_{-\pi}^{\pi} \frac{dK}{2\pi}\, \frac{e^{iKR}}{[(p+\gamma)^2 + 4u_K^2]^{1/2} - \gamma}; \tag{21}$$

$\epsilon > 0$ indicates that the integration contour is shifted to the right of the imaginary axis.

The corresponding Fourier transform gives the dynamic structure factor $S(\omega, \mathbf{k})$ accessible in scattering experiments. Namely, $S(\omega, \mathbf{k}) = G_{00}(i\omega, K)$, where the real-space wave-vector is $\mathbf{k} = \hat{\mathbf{z}}K/d$, assuming the chain is along the z-axis and the lattice constant is d.

2. Dynamics of a domain wall

The solution of Eq. (13) for a general K in the case of a domain wall, $V_s = \gamma\,|s|$, is only slightly more complicated. We only consider the case where the density matrix at $t = 0$ is diagonal, $\phi_s(t = 0, K) = \delta_{s,0}$. Due to the reflection symmetry of Eq. (13), the solution remains symmetric at all times, $\phi_s(t, K) = \phi_{-s}(t, K)$. As a result, we only need to consider $s \geq 0$. Denoting $g_s \equiv g_s(p, K)$ the Laplace transform of $\phi_s(t, K)$, with $\phi_s(0, K) = \delta_{s,0}$, we have the following algebraic equations:

$$pg_0 - 1 = -2iu_K g_1, \tag{22}$$

$$pg_s = -iu_K(g_{s-1} + g_{s+1}) - \gamma s g_s, \quad s > 0. \tag{23}$$

The system (23) being tri-diagonal, at a generic p there are only two linearly-independent solutions. If we introduce rescaled parameters, $z \equiv 2u_K/\gamma$ and $\nu = p/\gamma$, these equations are readily rendered into the form of Bessel recurrence relations for functions $Z_{\nu+s}(-iz)$. Then, the corresponding general solution of Eqs. (23) is

$$g_s = A\, e^{-is\pi/2} I_{\nu+s}(z) + B\, e^{is\pi/2} K_{\nu+s}(z), \tag{24}$$

where $I_\nu(z)$ and $K_\nu(z)$ are the modified Bessel functions of the first and second kind, respectively.

In lieu of guessing, we note that Eqs. (23) are finite-difference equations with coefficients linearly dependent on the index. Such and more general difference-differential equations can be solved with a version[22,23] of the Laplace's method for ordinary differential equations with coefficients linearly dependent on the independent variable[24]. In the case of Eq. (23), the corresponding solution is given by the complex integral,

$$g_s = \int_C dx\, e^{(\nu+s)x + iz\sinh x}, \tag{25}$$

where z and ν are defined as in Eq. (24), and the integration contour C must be chosen so that (i) the integral be non-zero, and (ii) the integrand returns to the same value at the ends of the contour (or returns to zero in an infinite contour). Recognizing Eq. (25) as a Sommerfeld integral representation[25] for modified Bessel functions of order $\nu + s$, up to a phase factor, we recover Eq. (24).

Only the first of the two solutions (24) falls to zero as $s \to +\infty$ at a fixed $z \neq 0$, which gives $B = 0$. The coefficient A is found with the help of Eq. (22), and the final result is

$$g_s(p) = e^{-i|s|\pi/2} \frac{I_{p/\gamma+|s|}(z)}{\gamma z\, I'_{p/\gamma}(z)}, \quad z = \frac{2u_K}{\gamma}, \quad s \in \mathbb{Z}, \tag{26}$$

where $I'_\nu(z) = I_{\nu+1}(z) + (\nu/z)I_\nu(z)$ is the derivative with respect to the argument. Using the appropriate asymptotic forms[26] of the modified Bessel functions, it is easy to check that the solution (26) goes to zero rapidly as s increases, and also that in the limit $\gamma \to 0$ the correct form in the absence of dephasing is recovered.

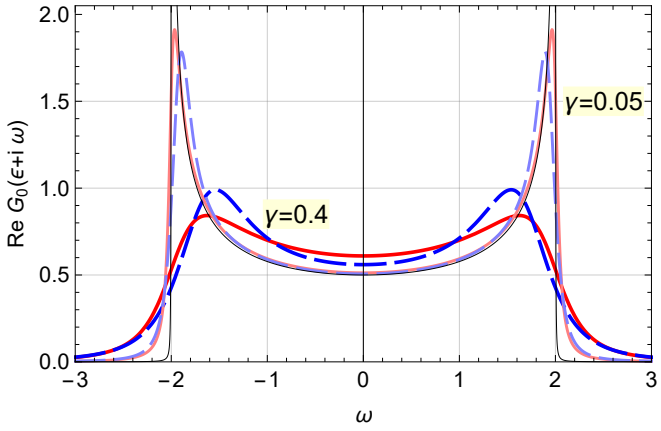

FIG. 2. (Color online) Frequency dependence of the real part of the dynamic structure factor for a particle [$G_{00}(\epsilon + i\omega, K)$, Eq. (20), red solid lines] and for a domain wall [$g_0(\epsilon + i\omega, K)$, see Eq. (26), blue dashed lines] with $u_K = 1$ and dephasing γ as labeled. The thin black line shows the corresponding result in the absence of dephasing. A regularization parameter $\epsilon = 10^{-3}$ was used for all the curves.

3. *Numerical comparison of the two cases*

In Eq. (13), the dependence on the dimensionless momentum K is encoded via the effective hopping u_K, which can be scaled away by the choice of time units and the corresponding rescaling of the dephasing rates V_s. Thus, in the following numerical examples, we only considered the case $u_K = 1$. In Fig. 2, we compare the structure factor for a particle, $G_{00}(\epsilon + i\omega, K)$ [Eq. (20)] and the corresponding quantity $g_0(\epsilon + i\omega)$ for a domain wall, Eq. (26). Clearly, the shape of the peaks is very similar between the two cases, even at relatively large values of γ.

Correspondingly, the real-time/space correlation functions $P(R, t)$ [see Eq. (21)] are also very similar. The inverse Laplace transform being numerically expensive, we computed $P(R, t)$ for the two cases by directly solving Eqs. (1) on finite-length chains, starting with a state localized on a single site in the middle of the chain. At $\gamma = 0$, our numerical solutions on chains of length $L = 25$ (not shown) are indistinguishable from the corresponding analytical solution on an infinite chain, $P_{\gamma=0}(R, t) = J_R^2(\Delta\, t)$, given in terms of the order-R Bessel function (thin black lines in Fig. 3). Numerical solutions for $R = 0, 1, 2$ and $\gamma = 0.05$, 0.1, and 0.4 are shown in Fig. 3. Again, the solutions for the two cases are very similar.

This is expected: as wave packet spreads, the density can be more and more accurately described by a low-order polynomial. Thus, according to our arguments in Sec. III A, the far-off-diagonal matrix elements of the density matrix rapidly get smaller, and so does the difference between the cases of a particle and a domain wall.

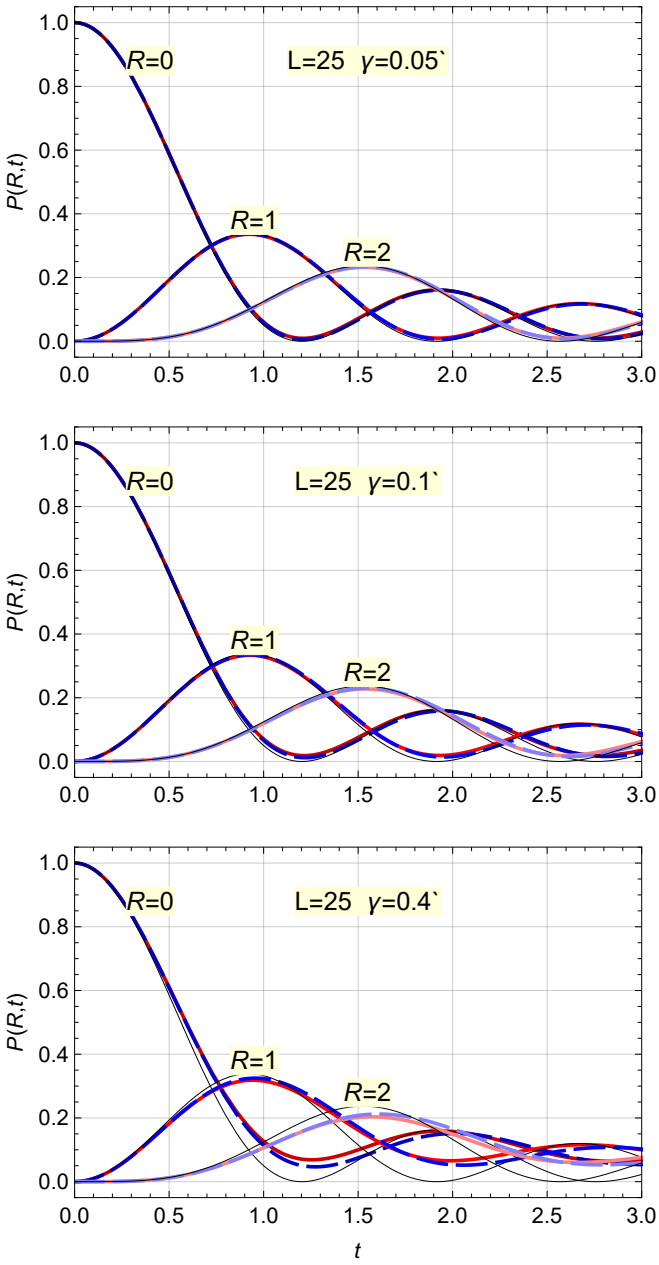

FIG. 3. (Color online) Time dependence of the probabilities $P(R, t)$, $R = 0, 1, 2$, for a particle (red solid lines) and for a domain wall (blue dashed lines) with $\Delta = 2$ and dephasing γ as indicated, in chains of length $L = 25$. The thin black line shows the corresponding result in the absence of dephasing, $P(R, t) = J_R^2(\Delta\, t)$, where $J_R(z)$ is the Bessel function of order R. Even for the largest dephasing, $\gamma = 0.4$, the particle and domain wall curves remain close to each other.

C. AC response spectrum of a finite chain

We now consider modified dynamics in the presence of an AC driving field. Physically, in the case of a charged particle, the driving field can be applied as an electric field along the chain direction. Similarly, in the case of a domain wall, it can be applied as a magnetic field in the easy-axis direction in the ferromagnetic case, or a gradient of such a field in the antiferromagnetic case.

The driving Hamiltonian $H_1 \equiv H_1(t)$ corresponds to a linear potential,

$$(H_1)_{ab} = -f(t)\, a\, \delta_{ab}, \quad \text{(no summation!)} \tag{27}$$

where, e.g., in the case of a charged particle in the electric field, the coefficient is $f(t) = e\mathcal{E}(t)\, d$, with e the charge and d the distance between neighboring sites, and we only consider harmonic driving fields, $\mathcal{E}(t) = \Re\mathrm{e}\, \mathcal{E}_0 e^{-i\omega t}$. The corresponding observable is the current (10), written here as an operator in the coordinate representation

$$J_{ab} = i\frac{\Delta}{2}\left(\delta_{a,b+1} - \delta_{a+1,b}\right), \tag{28}$$

the canonical current associated with the hopping Hamiltonian (2). We will compute the average current, the expectation of the current operator (28),

$$I(t) = \mathrm{Tr}[\hat{J}\rho(t)] \equiv \Re\mathrm{e}[Y(w)\mathcal{E}_0 e^{-i\omega t}], \tag{29}$$

where $Y(\omega)$ is the complex admittance whose real part is proportional to the absorption spectrum.

We note that the scattering mechanism considered here disregards transitions between the states of the chain with emission/absorption of bath excitations, which are normally responsible for the formation of the equilibrium Boltzmann distribution,

$$\rho^{(0)} = Z^{-1}\exp(-\beta H_0), \tag{30}$$

where Z is the normalization; at $\beta\Delta \ll 1$, on a chain of length L, one can use $Z \approx L$. This distribution is formed by other scattering processes. The rates of the corresponding transitions are small compared to the dephasing rate γ in the considered case $\beta^{-1} \gg \Delta, \gamma$.

Thus, we can still use the quantum kinetic equation (1) to analyze the absorption spectrum in this regime. Namely, in the presence of the perturbation Hamiltonian, $H = H_0 + H_1(t)$, we expand the density matrix around the equilibrium solution (30), $\rho = \rho^{(0)} + \rho^{(1)} + \ldots$, and solve only the equations for the perturbation linear in the applied field, $\rho^{(1)} \equiv \rho^{(1)}(t)$:

$$\dot{\rho}^{(1)}_{ab} + i[H_0, \rho^{(1)}]_{ab} + \Gamma_{ab}\rho^{(1)}_{ab} = -i[H_1(t), \rho^{(0)}]_{ab}. \tag{31}$$

Features of the absorption spectrum are most pronounced for short chains, and at sufficiently small $\gamma \ll \Delta$. Here the energy levels of the system in the absence of bath coupling, E_m, are well separated, so that the transition frequencies $\omega_{m-n} = E_m - E_n$ can be large compared to γ. In the absence of other transitions at the same frequency, at driving frequencies ω close to ω_{m-n}, the solution of Eq. (31) is dominated by only one resonant term, the matrix element $\rho^{(1)}_{mn}$. This results in a conventional Lorentzian line shape, with the complex admittance $Y(\omega) \propto (\omega - \omega_{m-n} + i\Gamma_{m-n})^{-1}$, where Γ_{m-n} is the dephasing rate for the energy-basis matrix element ρ_{mn}. As Weisskopf and Wigner realized early on[27], the line shape could be different if there are two or more pairs of levels corresponding to the same transition frequency ω_{m-n}. This effect, often called interference of transitions, is particularly common in weakly non-linear oscillators whose spectra are close to being equidistant[28].

Both situations occur for the transitions on a finite chain. Indeed, in the case of the hopping Hamiltonian (2) on a chain of length L, with zero boundary conditions, the energy levels are $E_m = -\Delta\cos k_m$, corresponding to the wave functions $\psi_m(a) = [2/(L+1)]^{1/2}\sin(k_m a)$ with $k_m = \pi m/(L+1)$, where both the site a and the energy index m are in the range $1, 2, \ldots, L$. The transition frequency is non-degenerate only in the symmetrical case, $m = L+1-n$. On the other hand, for any pair of energy states with indices m, n such that $m+n \neq L+1$, there is always a symmetric pair $m' = L+1-n$, $n' = L+1-m$ with the same transition frequency, $\omega_{m-n} = \omega_{m'-n'}$.

To calculate the corresponding admittance of a chain, notice that to leading order in powers of $\beta\Delta$ the r.h.s. of Eq. (31) is proportional to the current operator (28):

$$-i[H_1, \rho^{(0)}] \approx -iL^{-1}\beta[H_0, H_1] = \frac{\beta e d}{L}\mathcal{E}(t)\hat{J}. \tag{32}$$

Recalling that $\mathcal{E}(t) = \Re\mathrm{e}\, \mathcal{E}_0 e^{-i\omega t}$, let us introduce the dimensionless coupling constant $M \equiv \beta e \mathcal{E}_0 d/L$ and the small frequency bias $\nu \equiv \omega - E_m + E_n$. Then, as long as both ν and γ remain small compared to all transition frequencies, in the degenerate case $m+n \neq L+1$, the density matrix $\rho^{(1)}$ will have only two relatively large matrix elements in the energy basis, with the complex amplitudes $\phi_0 \equiv \rho^{(1)}_{mn}$ and $\phi_1 \equiv \rho^{(1)}_{m'n'}$. The corresponding secular equations read

$$\begin{cases} -i\nu\phi_0 + \Gamma_{mn,mn}\phi_0 + \Gamma_{mn,m'n'}\phi_1 &= MJ_{mn}, \\ -i\nu\phi_1 + \Gamma_{m'n',mn}\phi_0 + \Gamma_{m'n',m'n'}\phi_1 &= MJ_{m'n'}. \end{cases} \tag{33}$$

The coefficients are the matrix elements of the dephasing operator $\hat{\Gamma}$ [cf. Eq. (5)] in the energy basis,

$$\Gamma_{mn,m'n'} = \sum_{a,b}\psi_m(a)\psi_{m'}(a)\psi_{n'}(b)\psi_n(b)\, V_{a-b}, \tag{34}$$

and the matrix elements $J_{mn} \equiv \langle m|\hat{J}\,|n\rangle$ of the current operator (28). Only off-diagonal, $m \neq n$, matrix elements of the current operator are non-zero. Explicitly,

$$\begin{aligned} J_{mn} &= i\frac{\Delta}{2}\sum_{a=1}^{L-1}[\psi_m(a+1)\psi_n(a) - \psi_m(a)\psi_n(a+1)] \\ &= \frac{i\,\Delta}{L+1}\left(1 - e^{i\pi(m-n)}\right)\frac{\sin k_m \sin k_n}{\cos k_m - \cos k_n}. \end{aligned} \tag{35}$$

In particular, this gives a selection rule, $J_{mn} = 0$ for $m - n$ even. Also, for any pair of degenerate transitions, $\omega_{m-n} = \omega_{m'-n'}$, we have $J_{m'n'} = J_{mn}$. Similarly, we get the diagonal and the off-diagonal matrix elements (34) equal, $\Gamma_0 \equiv \Gamma_{mn,mn} = \Gamma_{m'n',m'n'}$ and $\Gamma_1 \equiv \Gamma_{mn,m'n'} = \Gamma_{m'n',mn}$. As a result of this symmetry, only the symmetric combination $\phi_0+\phi_1$ is excited by the external drive. Consequently, even in the degenerate case, the absorption peak retains the Lorentzian form, with half-width at half maximum $\Gamma_{m-n} = \Gamma_0 + \Gamma_1$.

Explicitly, in the case of a particle we obtain

$$\Gamma_0^{(\mathrm{P})} = \frac{L\gamma}{L+1}, \quad \Gamma_1^{(\mathrm{P})} = -\frac{\gamma}{L+1}, \tag{36}$$

which gives the peaks width $\Gamma^{(\mathrm{P})}_{m-n} = (L-1)\gamma/(L+1)$, $m+n \neq L+1$. In the non-degenerate case, $m+n = L+1$, we get $\Gamma^{(\mathrm{P})}_{m-n} = (2L-1)\gamma/(2L+2)$. By the selection rules ($m-n$ has to be odd), this transition is only allowed on even-length chains. As expected, in both cases, the line widths are close to γ.

In the case of a domain wall, after some tedious but elementary calculations, we obtain, in the degenerate case $m+n \neq L+1$:

$$\Gamma_0^{(\mathrm{DW})} = \gamma\,\frac{2(L+1)^2 + 1 - 3\csc^2 k_m - 3\csc^2 k_n}{6(L+1)}, \tag{37}$$

$$\Gamma_1^{(\mathrm{DW})} = -\gamma\,\frac{1}{L+1}\,\frac{1+\cos k_m \cos k_n}{(\cos k_m + \cos k_n)^2}, \tag{38}$$

where $\csc k \equiv 1/\sin k$ is the cosecant. In the non-degenerate case, $m+n = L+1$, we obtain

$$\Gamma^{(\mathrm{DW})}_{m-n} = \gamma\frac{4(L+1)^2 + 2 - 15\csc^2 k_m}{12(L+1)}. \tag{39}$$

Clearly, in these cases, the absorption line widths scale *linearly* with L. Given that the distances between the lines (say, for $m-n=1$) scale inversely proportionally to L, one expects that in the case of a domain wall individual peaks would cease to resolve at a smaller γ (with chain length L fixed).

In addition to degenerate perturbation theory analysis of a single absorption peak, we also solved numerically the full set of linear response equations (31) in the frequency domain, and computed the resulting admittance $Y(\omega)$. Numerical plots of the corresponding real part, $\chi(\omega) = \Re\mathrm{e}\, Y(\omega)$, on a chain of length $L = 7$ for a particle and a domain wall are shown in Fig. 4. As expected, only the absorption lines corresponding to the allowed transitions with $m-n$ odd are present. At small γ, we verified the predicted widths of the Lorentzian line shapes by fitting with the numerical data (not shown). It is clear from Fig. 4 that the discrete energy levels are much broader in the case of a domain wall, and individual absorption lines cease to be resolved at much smaller values of γ.

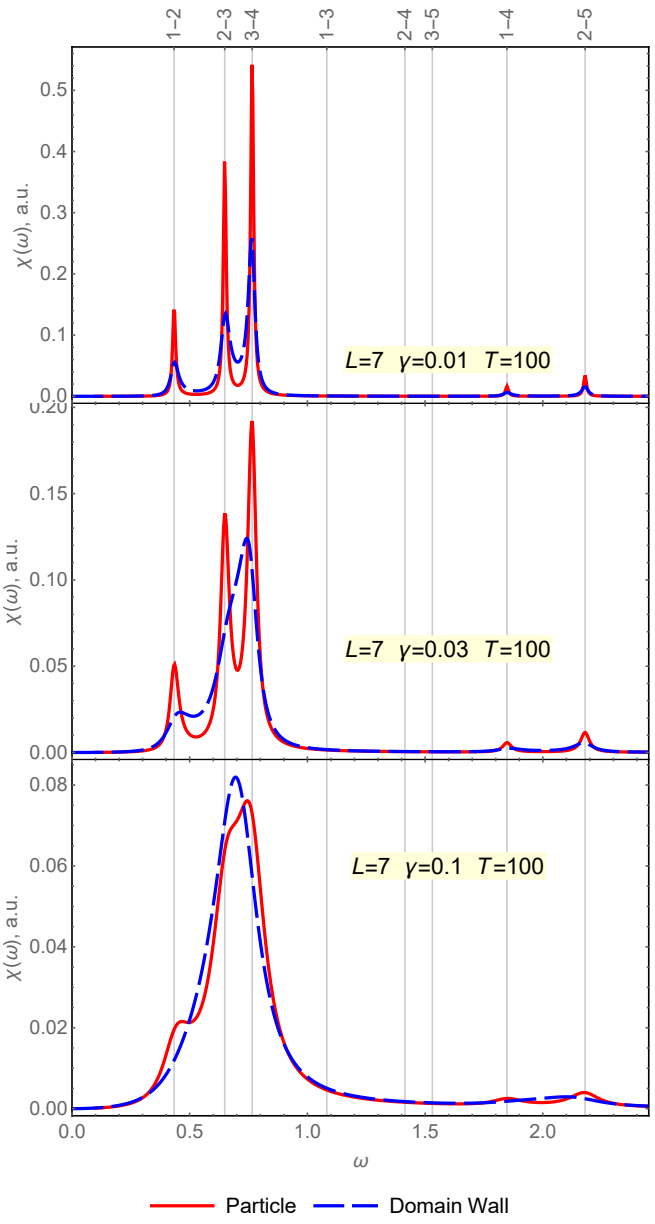

FIG. 4. (Color online) Frequency-dependent susceptibility $\chi(\omega) \equiv \Re\mathrm{e}\, Y(\omega)$ for a particle (red solid lines) and for a domain wall (blue dashed lines) on a chain of length $L = 7$ with the hopping parameter $\Delta = 2$ and dephasing γ as indicated. Vertical grid lines indicate the differences for pairs of discrete energy levels in the absence of dephasing, as labeled on the top frame.

IV. POSSIBLE EXPERIMENTAL REALIZATIONS

The one-dimensional models solved here apply to a broad range of (quasi-)1D systems, which in turn provide a variety of different platforms to study the dynamics of domain walls and/or particles in the presence of environmental relaxation. This poses the challenge to

test our conclusions in a single system directly. Ideally, one would be able to study both (**1**) bulk transport of topological defects in long chains and (**2**) resolve their spectral signatures in short chains, with (**3**) enough uniformity in properties to ensure that line widths are not dominated by inhomogeneous broadening, and yet (**4**) a variety of lengths to enable finite-size scaling. Further, (**5**) the system has to be in the regime of quantum diffusion, (**6**) with our simple models applicable, meaning that correlations between the baths on neighboring sites should be weak, with the bath free of sharp spectral features which could interfere with the measurements; preferably, (**7**) one should be able to confirm the relaxation model in a pump-probe-type experiment. Finally, for direct comparison, (**8**) one would like to measure both single-particle and domain wall dynamics in the same system. In this section, we address a number of such systems, focusing on these eight items.

A. Bulk and surface lattice defects

Quantum diffusion was first discovered for dilute point defects in bulk quantum crystals, using nuclear magnetic resonance spectroscopy[4–6]. While similar physics is also expected to govern the transport of point topological defects like kinks in a dislocation[7], to our knowledge, these predictions have never been confirmed experimentally[29]. Even if they were, due to the long-range nature of the deformation associated with bulk dislocations, we do not expect simple models studied in Sec. II to apply directly.

Related experiments could be possible with adatoms or adatom clusters on clean crystalline surfaces. Dynamics of such systems can be studied using direct imaging tools such as scanning tunneling microscopy and field ion microscopy, as well as a variety of indirect scattering techniques[30]. In particular, a regime of quantum or quantum-assisted diffusion was reported for hydrogen and deuterium atoms on metallic surfaces[31–33]. One could conceivably use a technique similar to electron energy-loss spectroscopy from Ref. 34 to detect discrete energy levels of an atom trapped in a quantum corral[35] or other nano-scale pattern on the surface[36,37]. In our opinion, the biggest challenge of such an experiment would be the small energies involved; a similar experiment with a quantum-confined topological defect (e.g., in a chain of adatoms) would be even harder.

B. Villain mode in quantum spin chains

Topological defects (domain walls) are much more common in quantum spin chains. In fact, they are readily seen in inelastic neutron scattering experiments[13], due to a characteristic line shape predicted by Villain[12,38]. An obvious question would be to what extent today's capabilities can be used to obtain, e.g., the details of the temperature dependence of line shapes, in particular, due to quantum interference effects in finite-length chains.

Neutrons probe the domain walls by measuring the Fourier components of the spin-spin correlation function $\langle S_z(\mathbf{r},t)S_z(\mathbf{0},0)\rangle$. For a single domain wall on an infinite chain, the corresponding dynamical structure factor can be obtained from Eq. (26) by simple scaling,

$$S(\omega,\mathbf{k}) = \frac{g_0(i\omega,K)}{\sin^2(K/2)}, \quad \mathbf{k} = \hat{\mathbf{z}}K/d. \tag{40}$$

Such a form factor—a Fourier transform of the sign function—is generally associated with an Ising domain wall. As expected, dephasing leads to broadening of the singularities in the Villain mode spectrum (see Fig. 2). Other broadening mechanisms include scattering between domain walls within a chain, as well as magnetic interactions with the domain walls in neighboring chains.

Chain lengths can be controlled by non-magnetic substitutions on the magnetic sites[39]. In principle, the energy resolution of inelastic neutron scattering should be sufficient to observe discrete energy levels for domain walls on finite-length chains. However, one would need to make sure that the inhomogeneous broadening due to different chain lengths does not swamp the decoherence-induced broadening.

Further, in the presence of a sufficiently strong magnetic field, one can cause the chains to undergo a spin-flop transition to a ferromagnetic phase. Above this transition, domain walls are confined to move in pairs (effectively equivalent to single flipped spins—akin to a true point-like particle); these pairs become the new elementary excitations. This would allow one to study directly the differences between particles and domain walls discussed in Sec. III C, although the spin relaxation mechanisms could be quite different in these two phases.

Instead of the finite-length chains, one could also construct disordered chains, where a small fraction of the bonds have a somewhat smaller exchange energy, thus providing a confining potential for the domain walls.

Yet another possibility is to look at the discrete spectra of bound domain wall pairs under conditions similar to those of the experiment in $CoNb_2O_6$ (Ref. 40). Namely, in an ordered magnetic phase stabilized by weak interchain couplings, there is a linear confining potential between the pairs of domain walls on the same chain. Near the bottom of the domain-wall-hopping band, the corresponding discrete energy levels are well described by a two-body Schrödinger equation with quadratic kinetic energy and linear potential[40]. The level widths, especially near the bulk Curie temperature where the confining potential is weaker, could reflect the signature of increased fragility of bound states of domain walls to environmental decoherence discussed in the present work.

C. Molecular chains and retinal systems

Another system supporting one-dimensional solitons are conjugated polymers like polyacetylene[41]. The defining feature of such systems is that sp^2 hybridization leaves one unpaired electron per carbon atom. This causes the spin-Peierls instability, which breaks the translational symmetry spontaneously and results in a doubly-degenerate dimerized state at the charge neutrality point. In the non-interacting picture, such a state would be a gapped semiconductor. However, energetics of the system at small dopings is such that each additional charge binds to a domain wall between two different degenerate ground states, resulting in mobile excitations with fractional charge $e/2$, and the effective mass closer to the electron mass rather than the ionic mass, as would be naïvely expected. Upon doping, such molecular-chain polymers have bulk conductivities comparable to that of copper.

Related finite-size systems can be readily formed by chemical means. Particularly interesting from our point of view are homo- or heterocyclic aromatic molecules and ions formed by conjugated cycles of odd lengths L, whose ground states are near-equal superpositions of L resonance contributions[42], each necessarily containing a soliton. Examples with $L = 5$ are furan C_4H_4O and cyclopentadienyl anion $[C_5H_5]^-$, and with $L = 7$, borepin C_6H_7B and tropylium cation $[C_7H_7]^+$.

Unlike in the case of the simple hopping Hamiltonian (2), detailed analysis and interpretation of molecular spectra is notoriously difficult[43–47], in particular, since ground state configurations involve bonds that are significantly bent (with angles dependent on L), while electronic transitions are always dressed with non-linear phonon modes. The problem is further complicated by (usually unresolved) rotational levels, and additional inhomogeneous broadening due to different nuclear spin configurations[24]; both effects result in quasi-continuum spectra even in closed systems. We expect the analysis of the level broadening, e.g., due to nearby substrate to be even more complicated, even though the rotational degrees of freedom should not not be relevant in this case.

The situation is potentially simpler in open chains where longer chains can retain their linear forms and make scaling with L meaningful[48], so that the energies for the transitions of interest could be smaller. A notable example of open chains are the small light-harvesting molecules (chromophores) in retinal systems[17,49,50] (e.g., rhodopsin). Here it has been proposed that the exceptionally fast response time scales and high quantum yield may originate from coherent motion of elementary soliton excitations. Interestingly, it was argued that a rapid damping of the solitons is key to ensure high quantum yield in these systems[49], and understanding the role of dephasing is therefore paramount. At first sight, since solitons are reflected at chain ends[17], one may expect self-interference to occur, and induce the enhanced fragility characteristic of emergent vs. real particles discussed in this work.

D. Cold atom and cold ion systems

An experimental system where essentially all parameters can be accurately computed is offered by cold atom systems in optical traps[51]. Quantum diffusion (with spontaneous emission serving as the source of decoherence) was predicted long ago[52]. In such a regime, our results are directly relevant for instance to the motion of solitons in the Su-Schrieffer-Heeger model, which has been recently realised in momentum space using ^{87}Rb atoms[15].

For finite-chain spectroscopy of particles or domain walls, one could combine interacting 1D optical lattices[53] and a box-trap[54] at half-filling, to achieve an "antiferromagnetically ordered" state (in the occupation number). Small variations away from half filling then introduce domain walls that can be driven periodically by tilting the box-trap[55]. The absorbed energy could be inferred by measuring the real-space momentum distribution at different times during the cycle of the applied linear tilting potential. These experiments could be done either with an ensemble of 1D box traps, or with a single trap; preparation and detection of bosons at single site level is within present state of the art capability[56].

Yet another possibility is offered by a recent experiment[57], where solitons in a zigzag chain of Mg^+ ions have been observed.

E. Quantum simulators and qubit registers

Finally, one more promising platform is provided by quantum simulators. These could be based on systems as distinct as ensembles of nitrogen-vacancy spin impurities in diamond[14] recently used in the search for discrete time crystals, or pairs of distinct states of $^{40}Ca^+$ ions in optical traps[58]. Their main attraction is the great tunability, and the capacity to manipulate and read out the behavior of the system locally.

In particular, a quantum Ising spin chain of length around ten sites has been implemented in Ref. 58. The Ising interactions decay as a (tuneable) power law with the distance, localized excitations can be injected into the system, and arbitrary multi-particle correlation functions can be measured, which gives the ability to perform quantum state tomography. In particular, the decay of a single spin flip into a pair of propagating domain walls has been observed in Ref. 58. With the addition of a dephasing mechanism, e.g., due to quasi-elastic scattering by photons, this system would allow a direct comparison between our theory and experiment.

Even more tunability is permitted by qubit registers, which are, in effect, small quantum computers, and allow for arbitrary one- and certain two-qubit gates to be performed. Specific implementations, where around ten

qubits are presently available, include hyperfine levels in trapped atomic ions[59] and superconducting flux qubit registers[60]. Of course, with access to such a register, one can directly construct an n-qubit entangled cat state $(|00\ldots0\rangle + |11\ldots1\rangle)/\sqrt{2}$ and study its decay; such experiments were done nearly a decade ago[61].

A more satisfying alternative would be to implement many-body quantum dynamics directly. This can be done by decomposing the unitary evolution operator into a sequence of small-angle Trotter slices, each applied during a single time-step of the quantum circuit. For example, to simulate a transverse-field quantum Ising chain, a repeated cycle of three time steps is sufficient, with the first two steps used for odd-bond and even-bond ZZ rotations, and the third step for local X rotations. When Ising exchange constant is large, couplings between sectors with different numbers of domain walls are suppressed, so that a single domain wall will evolve into a superposition of states dominated by the single domain wall sector. A quantum X-Y chain can be similarly simulated. Here, kinematic constraints imposed by the form of the X-Y Hamiltonian preclude pair-creation of further excitations so that a single-site excitation $|0\ldots010\ldots0\rangle$ at $t = 0$ will likewise evolve like a single particle. Classical dephasing noise can also be readily implemented, by introducing small random Z-rotations on individual qubits.

V. OUTLOOK

In this work we have studied and contrasted transport for particles and domain walls on chains, in the setting of a simple effective model with Markovian dephasing. We have also discussed a number of physical realisations where our results are likely to be relevant and where one may be able to put this theory to the test experimentally.

A different, potentially even more interesting setting is provided by the systems that originally inspired this work—higher-dimensional topological magnets with pointlike excitations that propagate across a spin background. Here, again, the spin background is changed when a particle passes a given point. Drawing on our results, we expect that in presence of weak dephasing a mechanism similar to quantum diffusion will govern transport in the bulk. On the contrary, we expect single-particle bound states to be suppressed compared to the case of a real particle, and the level broadening to increase with the spatial extent of the state.

Superficially, self-energy for the pointlike excitations can be computed using the retraceable path approximation, similar to what was done for a hole in the antiferromagnet[62,63]. In the presence of weak dephasing, this could give a lower bound on the associated broadening of discrete energy levels. It is not clear at the moment what the corresponding effect would be in the transport setting. We should note that the usual coherent transport may be suppressed, e.g., in the case of spin ice, where Trugman loops[64] are forbidden. Related effects, e.g., ring exchange processes, may also be strongly modified by environmental decoherence. Further work is needed to fully understand the corresponding physical consequences on the stability of quantum spin liquid systems. One implication, however, is that coherent transport over distances of several lattice spacings needs not necessarily imply the existence of spectral features associated with coherent ring exchange processes involving a comparable number of sites.

In conclusion, we have studied the effect of coupling to an environment on the transport of particle-like and domain-wall like excitations which model broad classes of physical systems. In the dc transport in large systems, in spite of the strong difference in the underlying dephasing caused by the environment, the effect is similar for both types of excitations. However, in small systems we show that the broadening of resonant spectral lines is significantly different.

ACKNOWLEDGMENTS

We are grateful to Sasha Chernyshev, Petar Jurcevic, Stephen Nagler, and Bella Lake for useful discussions, to the latter in particular for alerting us to the Villain mode experiments. LPP and CC are grateful for the hospitality of MPIPKS, where the project originated. This work was supported in part by EPSRC Grant No. EP/K028960/1 and EPSRC Grant No. EP/M007065/1 (CC), by the Deutsche Forschungsge-meinschaft via SFB 1143 (RM), by the US ARO grant W911NF-14-1-0272 and the US NSF grant PHY-1416578 (LP).

Appendix A: Dephasing from a boson bath

1. Quantum kinetics of a particle

We write the Hamiltonian for the particle in Fig. 1(a) in the general form,

$$H = H_0 + H_\mathrm{b} + H_\mathrm{i}, \tag{A1}$$

as a sum of the hopping Hamiltonian (2) in second-quantized form, $H_0 = -(\Delta/2)\sum_a (c_a^\dagger c_{a+1} + \mathrm{h.c.})$, the bath Hamiltonian H_b, and the interaction Hamiltonian H_i:

$$H_\mathrm{b} = \sum_\mu \omega_\mu b_\mu^\dagger b_\mu, \quad H_\mathrm{i} = \sum_a \epsilon_a c_a^\dagger c_a, \tag{A2}$$

$$\epsilon_a = \sum_\mu f_\mu^{(a)} u_\mu + \frac{1}{2}\sum_{\mu,\nu} g_{\mu\nu}^{(a)} u_\mu u_\nu. \tag{A3}$$

Here c_a annihilates a particle (it does not matter whether bosonic or fermionic, since we only consider one particle) on site a, b_μ annihilates a bath mode (bosonic) with frequency ω_μ, and ϵ_a is the energy of the coupling which

includes terms linear and quadratic in the displacement

$$u_\mu = \frac{b_\mu + b_\mu^\dagger}{(2\omega_\mu)^{1/2}}. \tag{A4}$$

We consider the evolution of the system using the particle density matrix in the position representation, $\rho_{aa'} = \langle c_a^\dagger c_{a'}\rangle$. In the absence of hopping, $\Delta = 0$, the evolution of the matrix element $\rho_{aa'}$ is readily evaluated if we introduce the phase associated with the boson coupling energies (A3) in the interaction representation,

$$\phi_a(t) \equiv \int_0^t dt'\, \epsilon_a(t'), \tag{A5}$$

evaluated using the time-dependent boson operators $\tilde{b}_\mu(t) = b_\mu e^{-i\omega_\mu t}$. In the single-particle subspace, for $\Delta = 0$, we have the exact equality:

$$e^{-iHt} c_a^\dagger e^{iHt} = e^{-iH_{\rm b}t} T_t e^{-i\int_0^t dt'\,\epsilon_a(t')} c_a^\dagger e^{iH_{\rm b}t}, \tag{A6}$$

where T_t is the standard time-ordering operator. Combining with the corresponding conjugate for $c_{a'}$, in the leading-order Gaussian approximation we obtain

$$\begin{aligned} \rho_{aa'}(t) &= e^{-W_{aa'}(t)}\rho_{aa'}(0), \\ W_{aa'}(t) &= \int_0^t dt'' \int_0^{t''} dt'\, w_{aa'}(t''-t'), \\ w_{aa'}(t''-t') &\equiv \langle \epsilon_a'' \epsilon_a' + \epsilon_{a'}' \epsilon_{a'}'' - \epsilon_a'' \epsilon_{a'}'' - \epsilon_a'' \epsilon_{a'}' \rangle, \end{aligned} \tag{A7}$$

where, e.g., $\epsilon_a' \equiv \epsilon_a(t')$, and the T-ordering of products matches that of the original exponents. Assuming an equilibrium boson distribution, and working to the leading order in the couplings, we decompose the averages into contributions coming from one- and two-boson processes, respectively, $w_{aa'}(t) = w_{aa'}^{(1)}(t) + w_{aa'}^{(2)}(t)$:

$$w_{aa'}^{(1)}(t) = \sum_\mu \frac{\left| f_\mu^{(a)} - f_\mu^{(a')} \right|^2}{2\omega_\mu} (2n_\mu + 1)\cos(\omega_\mu t), \tag{A8}$$

$$\begin{aligned} w_{aa'}^{(2)}(t) = \sum_{\mu,\nu} \frac{\left| g_{\mu\nu}^{(a)} - g_{\mu\nu}^{(a')} \right|^2}{8\,\omega_\mu \omega_\nu} \\ \times \Big[(2n_\mu + 1)(2n_\nu + 1)\cos(\omega_\mu t)\cos(\omega_\nu t) \\ - \sin(\omega_\mu t)\sin(\omega_\nu t) \Big]. \end{aligned} \tag{A9}$$

Here $n_\mu \equiv [\exp(\beta\omega_\mu) - 1]^{-1}$ is the equilibrium boson occupation number and $\beta \equiv \hbar/k_B T$. Notice that the obtained Debye–Waller factors (A7) are time-symmetric; this results from an assumption that the averages involving $[f_\mu^{(a)}]^2$ and $[g_{\mu\nu}^{(a)}]^2$ do not depend on the site index a.

At time t large compared to the inverse temperature and to the inverse bath cutoff frequency ω_c^{-1} (here $\omega_c \equiv \max_\mu \omega_\mu$), both correlation functions are expected to be small due to rapid oscillations of the integrand. Here, we can evaluate the integral (A7) by changing variable $t' \to t'' - \tau$, integrating over t'', and subsequently extending the upper integration limit in τ to infinity,

$$W_{aa'}(t) = \int_0^t d\tau\,(t-\tau)\, w_{aa'}(\tau) = t\,\Gamma_{aa'} - \widetilde{\Gamma}_{aa'}. \tag{A10}$$

The resulting asymptotic dephasing rate $\Gamma_{aa'}$ is

$$\Gamma_{aa'} = \int_0^\infty dt'\, w_{aa'}(t'). \tag{A11}$$

As a result of time integration, the single-boson contribution (A8) is dominated entirely by low frequency modes,

$$\Gamma_{aa'}^{(1)} = \frac{\pi}{\beta} \sum_\mu \frac{\left| f_\mu^{(a)} - f_\mu^{(a')} \right|^2}{\omega_\mu^2} \delta(\omega_\mu). \tag{A12}$$

This is non-zero and finite only if the bath spectral function,

$$F_{aa'}(\omega) \equiv \frac{\pi}{2} \sum_\mu \frac{\left| f_\mu^{(a)} - f_\mu^{(a')} \right|^2}{\omega_\mu} \delta(\omega_\mu - \omega) \tag{A13}$$

is linear function of $\omega > 0$ near the origin, which corresponds to the case of Ohmic dissipation. A sub-linear form $F_{aa'}(\omega) \propto \omega^\alpha$ with $\alpha < 1$ results in a formally divergent dephasing rate $\Gamma_{aa'}$.

Notice that in the case of a bath formed by lattice phonons in two or three dimensions (substrate phonons), necessarily $\Gamma_{aa'}^{(1)} = 0$. Indeed, only acoustic phonons can contribute at small frequencies, and the coupling $f_\mu^{(a)}$ becomes nearly position-independent at small wavevectors $k_\mu \to 0$.

In comparison, the dephasing rates coming from the two-boson contribution (A9) is dominated by scattering,

$$\Gamma_{aa'}^{(\rm sc)} = \frac{\pi}{4} \sum_{\mu,\nu} \frac{\left| g_{\mu\nu}^{(a)} - g_{\mu\nu}^{(a')} \right|^2}{\omega_\mu^2} (n_\mu + 1)\, n_\nu\, \delta(\omega_\mu - \omega_\nu). \tag{A14}$$

In the case of acoustic phonons at 1 K (well below the Debye energy scale), assuming a speed of sound $s = 5 \times 10^5$ cm/s, the inverse temperature is $\beta = \hbar/k_B T = 7 \times 10^{-11}$ s, which corresponds to a correlation radius of about $l_c \equiv s\beta = 350$ Å. This radius gets smaller with increasing temperature. Relevant fluctuations in the thermal baths for sites separated by distances larger that l_c are uncorrelated. When l_c is smaller than the distance between two adjacent lattice sites, assuming that the corresponding modes are similar, we recover Eq. (3).

Having analyzed the exponential decay of the matrix elements, we can now restore the hopping Δ to recover the full master equation (1). The Markovian approximation is valid when ρ changes little on the scale of the bath correlation time $\tau_c \equiv \max(\beta, \omega_{\rm max}^{-1})$, that is for $\tau_c \Delta \ll 1$, $\tau_c \gamma \ll 1$.

A more accurate evolution equation which includes non-Markovian effects can be derived using time-dependent Green's functions in the Keldysh formalism[65–68], or the formalism by Konstantinov and Perel'[69], with the help of an appropriate resummation of the perturbation series[70,71].

2. Quantum kinetics of a domain wall

Similar arguments apply to the case of a domain wall, Fig. 1(b), where we label the position of the domain wall by integers, and the positions of the spins by half-integers. Assuming the Ising exchange energy to be bond-independent, we write the position-dependent part of the energy of the domain wall at a as:

$$\epsilon_a = \sum_{j\in\{1/2,3/2,\ldots\}} \frac{1}{2}(h_{a+j} - h_{a-j}). \tag{A15}$$

Reversing this map, we get $\epsilon_{a+1} - \epsilon_a = h_{a+1/2}$. With this result, we can start with the same general Hamiltonian terms (A1) and (A2), with the fluctuating magnetic fields at half-integer sites j [cf. Eq. (A3)]:

$$h_j = \sum_\mu \bar{f}_\mu^{(j)} u_\mu + \frac{1}{2}\sum_{\mu,\nu} \bar{g}_{\mu\nu}^{(j)} u_\mu u_\nu. \tag{A16}$$

These immediately lead to the analogs of Eqs. (A8) and (A9) for the one- and two-boson Debye-Waller factors. The resulting dephasing rates are:

$$\bar{\Gamma}^{(1)}_{aa'} = \frac{\pi}{\beta}\sum_\mu \frac{\left|\sum_j \bar{f}_\mu^{(j)}\right|^2}{\omega_\mu^2}\delta(\omega_\mu); \tag{A17}$$

$$\bar{\Gamma}^{(2)}_{aa'} = \frac{\pi}{4}\sum_{\mu,\nu} \frac{\left|\sum_j \bar{g}_{\mu\nu}^{(j)}\right|^2}{\omega_\mu^2}(n_\mu+1)n_\nu\delta(\omega_\mu-\omega_\nu), \tag{A18}$$

where the summation over j encompasses the half-integer positions of the spins in the interval between a and a', namely, $\min(a,a') < j < \max(a,a')$. As a result, the single-phonon contribution to the dephasing rate $\Gamma_{aa'}$ may no longer be identically zero, consistent with the arguments in Ref. 11, and larger $|a-a'|$ are now expected to result in increasing dephasing rates due to an increasing number of terms included in the sum. With the correlation between the local fields h_j decaying to zero, we get an asymptotically linear growth, recovering Eq. (4) when the local fields are uncorrelated and identically distributed.

The asymptotic dephasing rates are approximately constant for $t \gg \tau_c = \max(\beta, \omega_c^{-1})$. Thus, the Markovian equations (1) and (4) are applicable for $\tau_c\Delta \ll 1$, $\tau_c\gamma|m-m'| \ll 1$. However, dephasing leads to an exponential suppression of the far off-diagonal matrix elements of the density matrix. Thus, if we use the dephasing rate Eq. (4) for large $|m-m'|$, technically outside of the applicability range of the Markovian approximation, the corresponding error is expected to be exponentially small. With this in mind, we use the Markovian dephasing rates (4) for all matrix elements.

* cc726@cam.ac.uk
† leonid@ucr.edu

[1] A. F. Andreev and I. M. Lifshitz, "Quantum theory of defects in crystals," Zh. Eksp. Teor. Fiz. **56**, 2057 (1969), [Sov.-Phys. JETP **29**, 1107 (1969)].
[2] R. A. Guyer and L. I. Zane, "Mass fluctuation waves." Phys. Rev. Lett. **24**, 1325–1325 (1970).
[3] Yu. Kagan and L. A. Maksimov, "Theory of particle transfer in extremely narrow bands," Zh. Eksp. Teor. Fiz. **65**, 622 (1974).
[4] R. G. Richards, J. Pope, and A. Widom, "Evidence for isotopic impuritons in solid helium," Phys. Rev. Lett. **29**, 708–711 (1972).
[5] V. N. Grigor'ev, B. N. Esel'son, V. A. Mikheev, and Yu.E. Shul'man, "Quantum diffusion of He^3 impurities in solid He^4," ZhETF Pis. Red. **17**, 25–28 (1973), [JETP Lett., **17**, 16 (1973)].
[6] V. N. Grigoriev, B. N. Esel'son, V. A. Mikheev, V. A. Slusarev, M. A. Strzhemechny, and Yu. E. Shulman, "^{3}He impurity excitations in solid ^{4}He," Journal of Low Temperature Physics **13**, 65–79 (1973).
[7] A. F. Andreev, "Elementary excitations in quantum crystals," Zh. Eksp. Teor. Fiz. **68**, 2341 (1975), [Sov.-Phys. JETP **41**, 1170 (1975)].
[8] L. D. C. Jaubert and P. C. W. Holdsworth, "Signature of magnetic monopole and Dirac string dynamics in spin ice," Nature Physics **5**, 258 – 261 (2009).
[9] Yuan Wan and Oleg Tchernyshyov, "Quantum strings in quantum spin ice," Phys. Rev. Lett. **108**, 247210 (2012), 1201.5314.
[10] C. Castelnovo, R. Moessner, and S. Sondhi, "Spin ice, fractionalization, and topological order," Annual Review of Condensed Matter Physics **3**, 35–55 (2012).
[11] Boris Ischi, Michael Hilke, and Martin Dubé, "Decoherence in a N-qubit solid-state quantum register," Phys. Rev. B **71**, 195325 (2005).
[12] J. Villain, "Propagative spin relaxation in the Ising-like antiferromagnetic linear chain," Physica B+C **79**, 1 – 12 (1975).
[13] S. E. Nagler, W. J. L. Buyers, R. L. Armstrong, and B. Briat, "Propagating domain walls in $CsCoBr_3$," Phys. Rev. Lett. **49**, 590–592 (1982).
[14] Soonwon Choi, Joonhee Choi, Renate Landig, Georg Kucsko, Hengyun Zhou, Junichi Isoya, Fedor Jelezko, Shinobu

Onoda, Hitoshi Sumiya, Vedika Khemani, Curt von Keyserlingk, Norman Y. Yao, Eugene Demler, and Mikhail D. Lukin, "Observation of discrete time-crystalline order in a disordered dipolar many-body system," Nature **543**, 221–225 (2017), 1610.08057.

[15] E. J. Meier, A. A. Fangzhao, and B. Gadway, "Observation of the topological soliton state in the su-schrieffer-heeger model," Nat. Commun. **7**, 13986–6 (2016).

[16] A. J. Heeger, S. Kivelson, Schrieffer J. R., and W.-P. Su, "Solitons in conducting polymers," Rev. Mod. Phys. **60**, 781–850 (1988).

[17] F. L. J. Vos, D. P. Aalberts, and W. van Saarloos, "Su-schrieffer-heeger model applied to chains of finite length," Phys. Rev. B **53**, 14922–14928 (1996).

[18] E. B. Davies, "Markovian master equations," Comm. Math. Phys. **39**, 91 (1974).

[19] G. Lindblad, "On the generators of quantum dynamical semigroups," Commun. Math. Phys. **48**, 119 (1976).

[20] A. F. Ioffe and R. Regel, "Non-crystalline, amorphous and liquid electronic semiconductors," in *Progress in Semiconductors*, Vol. 4, edited by A. F. Gibson (Heywood and Co., Ltd, London, 1960) pp. 237–291.

[21] N. F. Mott, "Conduction in non-crystalline systems. X. Mobility and percolation edges," Philosophical Magazine **29**, 613–639 (1974).

[22] A. A. Mirolyubov, "The solution of a class of linear differential-difference equations," Mat. Sbornik N.S. **34(76)**, 357–384 (1954), [In Russian].

[23] Barbara G. Yates, "The linear difference-differential equation with linear coefficients," Transactions of the American Mathematical Society **80**, 281–298 (1955).

[24] See the Appendix of L. D. Landau and E. M. Lifshitz, *Quantum Mechanics: non-relativistic theory* (Pergamon Press, Oxford, NY, 1977).

[25] Arthur Erdelyi, ed., *Higher Transcendental Functions*, Vol. II (McGraw-Hill Book Company, New York, 1953) california Institute of Technology Bateman Manuscript Project.

[26] "NIST digital library of mathematical functions," (2016), F. W. J. Olver, A. B. Olde Daalhuis, D. W. Lozier, B. I. Schneider, R. F. Boisvert, C. W. Clark, B. R. Miller and B. V. Saunders, eds.

[27] V. Weisskopf and E. Wigner, "Berechnung der natürlichen linienbreite auf grund der diracschen lichttheorie," Zeitschrift für Physik **63**, 54–73 (1930).

[28] M. I. Dykman and M. A. Krivoglaz, "Theory of nonlinear oscillations interacting with a medium," in *Physics Reviews*, Soviet scientific reviews, Section A, Vol. 5, edited by I. M. Khalatnikov (Hardwood Academic, Chur, Switzerland, 1984) pp. 266–442.

[29] However, some experiments have been interpreted in terms of oscillatory motion of such kinks, see L. P. Mezhov-Deglin and S. I. Mukhin, "Oscillations of kinks on dislocation lines in crystals and low-temperature transport anomalies as a "passport" of newly-induced defects," Low Temperature Physics **37**, 806–811 (2011).

[30] See, e.g., in Grazyna Antczak and Gert Ehrlich, *Surface Diffusion: Metals, Metal Atoms, and Clusters* (Cambridge University Press, 2010).

[31] R. DiFoggio and R. Gomer, "Diffusion of hydrogen and deuterium on the (110) plane of tungsten," Phys. Rev. B **25**, 3490–3511 (1982).

[32] X. D. Zhu, A. Lee, A. Wong, and U. Linke, "Surface diffusion of hydrogen on ni(100): An experimental observation of quantum tunneling diffusion," Phys. Rev. Lett. **68**, 1862–1865 (1992).

[33] Eliza M. McIntosh, K. Thor Wikfeldt, John Ellis, Angelos Michaelides, and William Allison, "Quantum effects in the diffusion of hydrogen on Ru(0001)," The Journal of Physical Chemistry Letters **4**, 1565–1569 (2013), pMID: 24920996, http://dx.doi.org/10.1021/jz400622v.

[34] Ş. C. Bădescu, P. Salo, T. Ala-Nissila, S. C. Ying, K. Jacobi, Y. Wang, K. Bedürftig, and G. Ertl, "Energetics and vibrational states for hydrogen on Pt(111)," Phys. Rev. Lett. **88**, 136101 (2002).

[35] M.F. Crommie, C.P. Lutz, D.M. Eigler, and E.J. Heller, "Quantum corrals," Physica D: Nonlinear Phenomena **83**, 98 – 108 (1995).

[36] Kedong Wang, Chun Zhang, M. M. T. Loy, and Xudong Xiao, "Time-dependent tunneling spectroscopy for studying surface diffusion confined in nanostructures," Phys. Rev. Lett. **94**, 036103 (2005).

[37] C. Z. Zheng, C. K. Yeung, M. M. T. Loy, and Xudong Xiao, "Quantum diffusion of H on Pt(111): Step effects," Phys. Rev. Lett. **97**, 166101 (2006).

[38] F. Devreux and J. P. Boucher, "Solitons in Ising-like quantum spin chains in a magnetic field: a second quantization approach," J. Phys. France **48**, 1663–1670 (1987).

[39] S. E. Nagler, W. J. L. Buyers, R. L. Armstrong, and Ritchie R. A., "Static and dynamic spin correlations in the random onedimensional antiferromagnet $csco_xmg_{1-x}cl_3$," J. Phys. C: Solid State Phys. **17**, 4819–4835 (1984).

[40] R. Coldea, D. A. Tennant, E. M. Wheeler, E. Wawrzynska, D. Prabhakaran, M. Telling, K. Habicht, P. Smeibidl, and K. Kiefer, "Quantum criticality in an Ising chain: experimental evidence for emergent E8 symmetry," Science **327**, 177 (2010).

[41] A. J. Heeger, S. Kivelson, J. R. Schrieffer, and W.-P. Su, "Solitons in conducting polymers," Rev. of Mod. Phys. **60**, 781–850 (1988).

[42] Jonathan Clayden, Nick Greeves, Stuart Warren, and Peter Wothers, *Organic Chemistry*, 1st ed. (Oxford University Press, USA, 2000).

[43] Tajiri Akio and Hatano Masahiro, "The mcd spectrum of the tropylium cation," Bulletin of the Chemical Society of Japan **45**, 962–963 (1972).

[44] Ove Christiansen and Poul Jørgensen, "The electronic spectrum of furan," Journal of the American Chemical Society **120**, 3423–3430 (1998).

[45] E. V. Gromov, A. B. Trofimov, N. M. Vitkovskaya, J. Schirmer, and H. Köppel, "Theoretical study of the low-lying excited singlet states of furan," The Journal of Chemical Physics **119**, 737–753 (2003).

[46] E. V. Gromov, A. B. Trofimov, N. M. Vitkovskaya, H. Köppel, J. Schirmer, H.-D. Meyer, and L. S. Cederbaum, "Theoretical study of excitations in furan: Spectra and molecular dynamics," The Journal of Chemical Physics **121**, 4585–4598 (2004).

[47] Thomas G. Schmalz, Luis Serrano-Andrés, Vicenta Sauri, Manuela Merchán, and Josep M. Oliva, "A distance-dependent parameterization of the extended hubbard model for conjugated and aromatic hydrocarbons derived from stretched ethene," The Journal of Chemical Physics **135**, 194103 (2011).

[48] Laren M. Tolbert, "Solitons in a box: the organic chemistry of electrically conducting polyenes," Accounts of Chemical Research **25**, 561–568 (1992).

[49] F. Buda, H. J. M. de Groot, and A. Bifone, "Charge

localization and dynamics in rhodopsin," Phys. Rev. Lett. **77**, 4474–4477 (1996).
[50] D. P. Aalberts and H. F. Stabenau, "A vision for ultrafast photoisomerization," Physica A **389**, 2981–2986 (2010).
[51] Chih-Chun Chien, Sebastiano Peotta, and Massimiliano Di Ventra, "Quantum transport in ultracold atoms," Nature Physics **11**, 998–1004 (2015).
[52] Navinder Singh, "Controllable diffusion of cold atoms in a harmonically driven and tilted optical lattice: decoherence by spontaneous emission," Journal of Physics A: Mathematical and Theoretical **41**, 255001 (2008).
[53] S. Palzer, C. Zipkes, C. Sias, and M. Köhl, "Quantum transport through a tonks-girardeau gas," Phys. Rev. Lett. **103**, 150601–4 (2009).
[54] A. L. Gaunt, Schmidutz T. F., Gotlibovych I., R. P. Smith, and Z. Hadzibabic, "Emergence of a turbulent cascade in a quantum gas," Phys. Rev. Lett. **110**, 200406–5 (2013).
[55] N. Navon, A. L. Gaunt, R. P. Smith, and Z. Hadzibabic, "Emergence of a turbulent cascade in a quantum gas," Nature **539**, 72–75 (2016).
[56] Ott H., "Single atom detection in ultracold quantum gases: a review of current progress," Rep. Prog. Phys. **79**, 054401–(2016).
[57] J. Brox, P. Kiefer, M. Bujak, T. Schaetz, and H. Landa, "Spectroscopy and directed transport of topological solitons in crystals of trapped ions," Phys. Rev. Lett. **119**, 153602 (2017).
[58] P. Jurcevic, B. P. Lanyon, P. Hauke, C. Hempel, P. Zoller, R. Blatt, and C. F. Roos, "Quasiparticle engineering and entanglement propagation in a quantum many-body system," Nature **511**, 202 (2014).
[59] Kenneth R Brown, Jungsang Kim, and Christopher Monroe, "Co-designing a scalable quantum computer with trapped atomic ions," npj Quantum Information **2**, 16034 (2016).
[60] C. Neill, P. Roushan, K. Kechedzhi, S. Boixo, S. V. Isakov, V. Smelyanskiy, R. Barends, B. Burkett, Y. Chen, Z. Chen, B. Chiaro, A. Dunsworth, A. Fowler, B. Foxen, R. Graff, E. Jeffrey, J. Kelly, E. Lucero, A. Megrant, J. Mutus, M. Neeley, C. Quintana, D. Sank, A. Vainsencher, J. Wenner, T. C. White, H. Neven, and J. M. Martinis, "A blueprint for demonstrating quantum supremacy with superconducting qubits," (2017), [unpublished], arXiv:1709.06678.
[61] Rainer Blatt and David Wineland, "Entangled states of trapped atomic ions," Nature **453**, 1008–1015 (2008).
[62] M. M. Mohan, "Possibility of quasiparticle behaviour in the strongly correlated Hubbard model," Journal of Physics: Condensed Matter **3**, 4307 (1991).
[63] Oleg A. Starykh and George F. Reiter, "Hole motion in the ising antiferromagnet: An application of the recursion method," Phys. Rev. B **53**, 2517 (1996).
[64] S. A. Trugman, "Interaction of holes in a Hubbard antiferromagnet and high-temperature superconductivity," Phys. Rev. B **37**, 15971603 (1988).
[65] L. V. Keldysh, "Diagram technique fon non-equilibrium processes," Zh. Eksp. Teor. Fiz. **47**, 1515 (1964), [Sov. Phys. JETP **20**, 1018 (1965)].
[66] J. Rammer and H. Smith, "Quantum field-theoretical methods in transport theory of metals," Rev. Mod. Phys. **58**, 323–59 (1986).
[67] A. Kamenev, "Many-body theory of non-equilibrium systems," (2004), lectures notes for 2004 Les Houches Summer School on "Nanoscopic Quantum Transport", arXiv:cond-mat/0412296.
[68] Hartmut Haug and Antti-Pekka Jauho, *Quantum kinetics in transport and optics of semiconductors*, 2nd ed. (Springer, New York, 2008).
[69] O. V. Konstantinov and V. I. Perel, "A graphical technique for computation of kinetic quantities," Zh. Exp. Teor. Fiz. **39**, 197–208 (1960).
[70] M. I. Dykman, "Relaxation of impurities in a nonresonant field and phonon amplification," Fiz. Nizk. Temp. **5**, 186–97 (1979), [Soviet J. Low Temp. Phys. 5, pp. 89-95 (1979)].
[71] L. P. Pryadko and P. Sengupta, "Quantum kinetics of an open system in the presence of periodic refocusing fields," Phys. Rev. B **73**, 085321 (2006).